Multigrid Acceleration of Three Turbulence Models in Predicting Stratified Flow Driven by Natural Convection in a Square Cavity

[1*]Kiattisak Ngiamsoongnirn, [2]Varangrat Juntasaro and [1]Ekachai Juntasaro

[1]School of Mechanical Engineering, Institute of Engineering,
Suranaree University of Technology, Nakhon Ratchasima 30000, Thailand,
Tel: (+6644) 224410-2, *Email: kiatt2000@hotmail.com
[2]Department of Mechanical Engineering, Faculty of Engineering,
Kasetsart University, Bangkok 10900, Thailand,
Tel: (+662) 9428555 ext 1829, Email: fengvrj@ku.ac.th

Abstract: *This paper presents the implementation of three low-Reynolds-number turbulence models into the self-developed CFD code to simulate the thermally driven airflow due to natural convection inside a square cavity. The turbulence models selected in this work are the* $k-\varepsilon$ *model of Launder & Sharma (LS) [1], the SST* $k-\omega$ *model of Menter (SST) [2], and the* $\overline{v^2}-f$ *model of Durbin (V2F) [3]. The capability in prediction of each model is evaluated in terms of accuracy of the computed results compared to the experiment of Ampofo (EXP) [4] and the convergence behavior of each one will be discussed in details. To accelerate the rate of convergence, this paper adopts a multigrid technique to annihilate an improper error in each grid set.*

Keywords: Low-Reynolds-Number; Multigrid Acceleration; Natural Convection; Square Cavity

Nomenclature

a	Empirical constant in turbulence model
A	Matrix coefficient
B_f	Blending function in turbulent model
C_1, C_2, C_3, C_L, $C_{\varepsilon 1}$, $C_{\varepsilon 2}$, $C_{\varepsilon 3}$, C_η, C_μ	Empirical constant in turbulence model
d_n	Normal distance to the nearest wall
f	Intermediate variable in turbulence model
f_1, f_2, f_μ	Damping functions
g	Gravitational acceleration
G_B	Turbulent buoyancy production
h	Grid size
i, j	Direction coordinates
$I_a^b \phi^a$	Interpolation operator with the data ϕ^a transferred from a up to b
k	Turbulent kinetic energy
L	Width of cavity, turbulent length scale
p	Pressure
P_k	Turbulent production
Pr	Prandtl number [$=\nu/\alpha$]
Ra	Raleigh number [$=g\beta(T_H-T_C)L^3/(\alpha\nu)$]
S	Source term in general transport equation
T	Temperature, turbulent time scale
T_H, T_C	Hot and cold wall temperature respectively
T_{ref}	Reference temperature [$=(T_H+T_L)/2$]
u_j	Mean velocity components in j-direction
V_0	Buoyancy velocity [$=\sqrt{g\beta L(T_H-T_C)}$]
$\overline{v^2}$	Turbulent velocity scale
x_j	Coordinate in j-direction

Greeks

α	Thermal diffusivity
α, α_1, α_2, α^*	Empirical constant in turbulence model
β	Coefficient of thermal expansion
δ	Kronecker delta
μ	Molecular dynamic viscosity
μ_t	Eddy dynamic viscosity
ν	Molecular Kinematics viscosity [$=\mu/\rho$]
ε, $\tilde{\varepsilon}$	Dissipation rate of turbulent kinetic energy
ϕ	Independent variable in general transport equation, approximate solution
ρ	Fluid density
σ_k, σ_{k1}, σ_{k2}, σ_ε, σ_ω, $\sigma_{\omega 1}$, $\sigma_{\omega 2}$, σ_T	Turbulent Prandtl numbers
ω	Specific Dissipation rate of turbulent kinetic energy
Γ	Diffusion coefficient

1. Introduction

The cavity type of flow and heat transfer phenomena is encountered in many engineering practices, e.g. room heating, cooling of electrical and electronic equipment, crystal growth, flows in nuclear reactor and fire-induced smoke spread, etc. All these enclosure flows are commonly dominated by buoyancy and near wall effects. Although the geometry and boundary conditions of a cavity are so simply and can easily be implemented in numerical simulation. However, the phenomena of flow regarding free convection in a square cavity with two differentially heated vertical walls are somewhat complex and much more complex with increasing Raleigh number, $10^6 \le \mathrm{Ra} \le 10^{12}$. The core region is largely stratified and laminar. The rapid change of flow is trapped in the vicinity of the wall. In addition, the flow in this case might include simultaneously laminar, transition, and turbulent regions leading to none of turbulent model can predict correctly the whole flow field [4].

Over the past decades, several achievements in simulation of isothermal flows and non-isothermal convective flows using the two-equations turbulence model are presented in the literature. Only a few works have concerned with natural convection, especially free convection in a square enclosure, which is hardly tractable by the two-equations turbulence model at very high *Ra* [5]. Moreover, an attempt in using a multigrid technique to accelerate convergence rate does not appear in the literature. For this reason, it challenges to simulate a turbulent natural convection in a square cavity by using the two-equations turbulence model with the multigrid accelerator. This motivates the presence of the present work.

2. Governing Equations

2.1 Mean Flow and Energy Equations

The Reynolds-averaged Navier-Stokes equation and the time-averaged energy equation are considered in the present work. For a steady incompressible flow, the equations governing fluid flow and heat transfer can be expressed as follows:

the mean continuity equation

$$\frac{\partial}{\partial x_j}(\rho u_j) = 0\ ;$$

the mean momentum equation

$$\frac{\partial}{\partial x_j}(\rho u_j u_i) = -\frac{\partial p}{\partial x_i} + \frac{\partial}{\partial x_j}\left[\mu\left(\frac{\partial u_i}{\partial x_j} + \frac{\partial u_j}{\partial x_i}\right) - \rho\overline{u_i' u_j'}\right] - \rho g_i \beta (T - T_{ref})\ ;$$

and the mean energy equation represented by mean temperature equation

$$\frac{\partial}{\partial x_j}(\rho u_j T) = \frac{\partial}{\partial x_j}\left[\frac{\mu}{\mathrm{Pr}}\frac{\partial T}{\partial x_j} - \rho\overline{u_j' T'}\right].$$

This averaging process gives rise to the two unknowns: the Reynolds stress $\overline{u_i' u_j'}$ and the turbulent heat flux $\overline{u_i' T'}$. Based on the Boussinesq approximation, the Reynolds stress can be expressed as

$$\rho\overline{u_i' u_j'} = -\mu_t\left(\frac{\partial u_j}{\partial x_i} + \frac{\partial u_i}{\partial x_j}\right) + \frac{2}{3}\rho k \delta_{ij}\ ,$$

and with the standard gradient diffusion hypothesis, the turbulent heat flux is in the form

$$\rho\overline{u_j' T} = \frac{\mu_t}{\sigma_T}\frac{\partial T}{\partial x_j}\ ,$$

where g_i represent to g_x and g_y in which g_x is omitted and $g_y = -g = -9.81\ m/s^2$ which is the gravitational acceleration, and for ideal gas $\beta = 1/T_{ref}$.

2.2 Turbulence Modeling Equations

The Reynolds stress based on the Boussinesq approximation is related to the velocity gradient, the turbulent kinetic energy and the eddy viscosity. The eddy viscosity remains the unknown quantity, which needs further modeling. This leads to the eddy viscosity model. It is modeled relating to the turbulent quantities in which these turbulent quantities possess their own transport equations. There are several zero, one, two or more equations turbulence models proposed in the literature. The three low-Reynolds-number versions of two-equations turbulence models are considered in this work: $k-\varepsilon$, $k-\omega$ and $\overline{v^2}-f$. They can be described in detail as follows.

2.2.1. k - $\tilde{\varepsilon}$ Model of Launder and Sharma

The turbulent kinetic energy equation and the dissipation rate of turbulent kinetic energy equation are formulated respectively as

$$\frac{\partial}{\partial x_j}(\rho u_j k) = \frac{\partial}{\partial x_j}\left[\left(\mu + \frac{\mu_t}{\sigma_k}\right)\frac{\partial k}{\partial x_j}\right] + P_k + G_B - \rho(\tilde{\varepsilon} + D_k)$$

$$\frac{\partial}{\partial x_j}(\rho u_j \tilde{\varepsilon}) = \frac{\partial}{\partial x_j}\left[\left(\mu + \frac{\mu_t}{\sigma_\varepsilon}\right)\frac{\partial \tilde{\varepsilon}}{\partial x_j}\right] + \frac{C_{\varepsilon 1} f_1 (P_k + C_{\varepsilon 3} G_B)}{T} - \frac{\rho C_{\varepsilon 2} f_2 \tilde{\varepsilon}}{T} + E$$

where $\tilde{\varepsilon} = \varepsilon + 2\frac{\mu}{\rho}\left(\frac{\partial\sqrt{k}}{\partial x_j}\right)^2$ is modified to simplify the boundary condition for the dissipation rate of turbulent kinetic energy and the extra source term E is added to account for the near wall effect. The eddy viscosity and turbulent time scale are defined respectively as

$$\mu_t = \rho C_\mu f_\mu k T\ ,\ T = \frac{k}{\varepsilon}.$$

2.2.2 SST $k-\omega$ Model of Menter

In this model, the turbulent kinetic energy dissipation rate is altered to the specific one with the relation $\omega \sim \varepsilon / k$. The turbulent kinetic energy equation and its specific dissipation rate in this model are respectively expressed as

$$\frac{\partial}{\partial x_j}(\rho u_j k) = \frac{\partial}{\partial x_j}\left[\left(\mu + \sigma_k \mu_t\right)\frac{\partial k}{\partial x_j}\right] + P_k + G_B - \rho\alpha^* \omega k$$

$$\frac{\partial}{\partial x_j}(\rho u_j \omega) = \frac{\partial}{\partial x_j}\left[\left(\mu + \sigma_\omega \mu_t\right)\frac{\partial \omega}{\partial x_j}\right] + \frac{C_\omega}{\mu_t}(P_k + C_3 G_B) - \rho\alpha\omega^2$$

$$+ 2(1-B_f)\frac{\rho\sigma_\omega}{\omega}\frac{\partial k}{\partial x_j}\frac{\partial \omega}{\partial x_j}$$

The blending function B_f appeared in the $\omega-$equation, which blends the model coefficients of the $k-\omega$ model in boundary layers with the transformed $k-\varepsilon$ model in free-shear layers and free stream zones, is defined as

$B_f = \tanh(\arg_1^4)$,

where $\arg_1 = \min\left[\max\left(\frac{\sqrt{k}}{\alpha^* d_n \omega}, \frac{500\mu}{\rho d_n^2 \omega}\right), \frac{4\rho\sigma_{\omega 2} k}{CD_{k\omega} d_n^2}\right]$

and $CD_{k\omega} = \max\left(\frac{2\rho\sigma_{\omega 2}}{\omega}\frac{\partial k}{\partial x_j}\frac{\partial \omega}{\partial x_j}, 10^{-20}\right)$.

The eddy viscosity is modeled as

$$\mu_t = a\min\left(\frac{\rho k}{a\omega}, \frac{\rho k}{b\Omega}\right),$$

where $\Omega = \sqrt{\left(\frac{\partial v}{\partial x} - \frac{\partial u}{\partial y}\right)^2}$, $a = 0.31$, $b = \tanh(\arg_2^2)$,

and $\arg_2 = \max\left(\frac{2\sqrt{k}}{\alpha^* d_n \omega}, \frac{500\mu}{\rho d_n^2 \omega}\right)$.

2.2.3. $\overline{v^2}$ - f Model of Durbin

The $\overline{v^2}$ - f turbulence model is an alternative to the k - ε model and was introduced to model the near-wall turbulence without the use of exponential damping or wall functions [6]. The model requires the solution of four differential equations, two of which are the basic equations for k and ε which are the same those as Launder and Sharma model, including the eddy viscosity, with different turbulent time scale, extra terms and damping functions, and in addition $\tilde{\varepsilon}$ replaced with ε. The two additional equations are the transport equation of turbulent velocity scale and the helmoltz-like elliptic relaxation for intermediate equation f, which can be written as follows:

The turbulent velocity scale equation is in the form

$$\frac{\partial}{\partial x_j}(\rho u_j \overline{v^2}) = \frac{\partial}{\partial x_j}\left[\left(\mu + \frac{\mu_t}{\sigma_k}\right)\frac{\partial \overline{v^2}}{\partial x_j}\right] + \rho k f - 6\rho\overline{v^2}\frac{\varepsilon}{k},$$

The helmoltz-like elliptic relaxation for the intermediate variable f is formulated as

$$f - L^2\frac{\partial^2 f}{\partial x_i^2} = \frac{1}{T}\left[(C_1 - 1)\frac{2}{3} - (C_1 - 6)\frac{\overline{v^2}}{k}\right] + \frac{C_2}{k}(P_k + C_{3\varepsilon} G_B)$$

where the length scale L and the time scale T are defined respectively as

$$L^2 = C_L^2 \max\left[\frac{k^3}{\varepsilon^2}, C_\eta^2\sqrt{\frac{\nu^3}{\varepsilon}}\right],\ T = \max\left[\frac{k}{\varepsilon}, 6\sqrt{\frac{\nu}{\varepsilon}}\right].$$

2.2.4 Initial and Boundary Conditions

To initiate the guessed value of the considering variables, the initial velocity and temperature in all models are specified with stagnant velocity and mean temperature averaged between the hot and cold walls temperature, respectively. The turbulent kinetic energy and turbulent dissipation rate or specific turbulent dissipation rate are specified such that the order of eddy viscosity is much more than the order of molecular viscosity. This paper specifies as follows: $k = 10^{-3}$, $\tilde{\varepsilon} = \varepsilon = 10^{-5}$, and $\omega = 10^{-3}$. In case of $\overline{v^2} - f$ model, the turbulent velocity scale $\overline{v^2}$ and an intermediated variable f are set as $\overline{v^2} = f = 10^{-3}$.

In regard to the boundary conditions, the no-slip condition is applied at all sides of the wall resulting a known boundary condition for velocity. For temperature, the left vertical wall is heated with constant temperature at $T_H = 50\ ^\circ C$ and the right one is cooled at $T_C = 10\ ^\circ C$. The upper and lower horizontal wall are linearly interpolated between the left and right vertical ones. To set the boundary conditions for the turbulent quantity and relevant variables, different models are set in different ways. They are specified as follows:

$k-\varepsilon$ *Model of Launder and Sharma*: $k = \tilde{\varepsilon} = 0$;

SST $k-\omega$ *Model of Menter*: $k = 0$, $\omega = \frac{60\mu}{\rho\alpha_1 d_1^2}$;

$\overline{v^2} - f$ *Model of Durbin*: $k = \overline{v^2} = f = 0$, $\varepsilon = \frac{2\mu k}{\rho d_1^2}$;

where d_1 is the distance from the wall next to the first node.

2.2.5 The Model Constants and Damping Functions

It is clearly apparent that there is the common terms appeared in all models. They are the turbulent production term P_k and the buoyancy production term G_B. Their definition are expressed as

$$P_k = \mu_t \left[2\left(\frac{\partial u}{\partial x}\right)^2 + 2\left(\frac{\partial v}{\partial y}\right)^2 + \left(\frac{\partial v}{\partial x} + \frac{\partial u}{\partial y}\right)^2 \right],$$

$$G_B = -\frac{\mu_t g \beta}{\sigma_T}\frac{\partial T}{\partial y}.$$

Besides the common terms, there are several empirical constants, damping functions and extra source terms. In each models, they are set in different values as follows:

$k-\varepsilon$ Model of Launder and Sharma:

$\sigma_k = 1.0,\ \sigma_\varepsilon = 1.3,\ \sigma_T = 0.9$,

$C_\mu = 0.09,\ C_{\varepsilon 1}=1.44,\ C_{\varepsilon 2} = 1.92,\ C_{3\varepsilon} = \tanh\left(\left|\frac{v}{u}\right|\right)$

$f_1 = 1.0, f_2 = 1.0 - 0.3e^{-Re_t^2}, f_\mu = e^{-3.4/(1+0.02Re_T)^2}$,

$$D = 2\mu\left(\frac{\partial\sqrt{k}}{\partial x_j}\right)^2,\ E = 2\rho\nu\nu_t\left(\frac{\partial^2 u_i}{\partial x_j \partial x_k}\right)^2.$$

SST $k-\omega$ Model of Menter:

The model constants of the SST turbulence model, C_ω, α, σ_k and σ_ω, are obtained by blending the model constants of the $k-\omega$ model, denoted as ϕ_1, with those of the transformed high-Re-number $k-\varepsilon$ model (ϕ_2). The resulting relation becomes

$$\phi = B_f\phi_1 + (1-B_f)\phi_2,$$

where B_f, the blending function, is just defined in the above section.

The model constants of the $k-\omega$ model are
$\alpha_1 = 0.075$ $\sigma_{k1} = 0.85$, $\sigma_{\omega 1} = 0.5$, and $C_{\omega 1} = 0.533$.
And the model constants of the $k-\varepsilon$ model are
$\alpha_2 = 0.0828$, $\sigma_{k2} = 1.0$, $\sigma_{\omega 2} = 0.856$, and $C_{\omega 2} = 0.44$.

$\overline{v^2} - f$ Model of Durbin:

$\sigma_k = 1.0$, $\sigma_\varepsilon = 1.3$, $\sigma_T = 0.9$,

$C_{\varepsilon 1} = 1.4$, $C_{\varepsilon 2} = 1.9$, $C_{3\varepsilon} = \tanh\left(\left|\frac{v}{u}\right|\right)$,

$C_1 = 1.4$, $C_2 = 0.3$, $C_\eta = 70$, $C_\mu = 0.19$, $C_L = 0.3$,

$f_1 = \left(1 + 0.045\sqrt{k/\overline{v^2}}\right)$, $f_2 = 1.0$, $f_\mu = \overline{v^2}/k$, $E = D = 0$.

3. Numerical Method

The governing equations are in the form of partial differential equation and can be written in general transport form as

$$\frac{\partial}{\partial x_j}(\rho u_j \phi) = \frac{\partial}{\partial x_j}\left(\Gamma^\phi \frac{\partial \phi}{\partial x_j}\right) + S^\phi$$

To solve this equation with the use of computer simulation, it is necessary to convert the partial differential equation form into an algebraic form of equation. This is the so-called discretization process. This paper uses the finite volume formulation to discretize the governing equations based up on a structural non-staggered Cartesian grid system. The discretized equations written in the standard finite volume formulation become

$$a_P\phi_P = \sum_{n=E,W,N,S} a_n\phi_n + S^\phi.$$

The resulting algebraic equations are solved with a segregated manner. The SIMPLE algorithm is adopted in this work to couple the system of equations. Each algebraic equation is solved iteratively by an alternating line-by-line TDMA. The multigrid algorithm, as will be discussed in the next section, is employed to accelerate convergence rate. The convection and diffusion terms are respectively interpolated with typical first order upwind and second order central schemes. Even though the developed CFD code in this work has built-in the QUICK convection scheme, but it is treated not available because it takes too much computing time when including QUICK convection scheme and it does not significantly improve solution accuracy for this case. The solution accuracy is rather depend on the number of grid points in the vicinity of the wall than a truncation error order of the scheme used. As a result, it seems not to worth in including QUICK convection scheme.

4. Multigrid Methodology

In the multigrid method the computation is carried out on a number of grids set with different grid size *h*, the finest grid is denoted by h and each level of the coarse grids is represented by multiplying an integer number, i.e., *2h, 3h, 4h* and so on. The exact solution for any variable ϕ^h on grid level h satisfies the following equation:

$$A^h\phi^h = S^h.$$

Unless the approximate solution satisfies the exact solution and boundary conditions, the equation will contain a residual R^h given by

$$A^h\tilde{\phi}^h = \tilde{S}^h - R^h,$$

where the approximate solution is denoted by the superscript '~'. The exact and approximate solutions are related each other with $\phi^h = \tilde{\phi}^h + e^h$, where e^h is the correction of an approximate solution. By subtracting the approximate equation from the exact equation, the result becomes

$$A^h(\tilde{\phi}^h + e^h_\phi) - A^h\tilde{\phi}^h = S^h - \tilde{S}^h + R^h.$$

To determine the correction e^h_ϕ, the approximate solutions $\tilde{\phi}^h$ on grid level h is transferred onto the coarser grid level $2h$:

$$A^{2h}(I_h^{2h}\phi^h + e_\phi^{2h}) - \hat{A}\tilde{\phi}^{2h} = \tilde{S}^{2h} - \hat{S}^{2h} + I_h^{2h}R^{2h},$$

this is the restriction process, where the super script '^' denotes the information calculated from the restricted solutions. Moving the known quantities to the right-hand side, the equation is reduced to

$$A(\tilde{\phi}^{2h}) = \hat{C}^{2h} + \tilde{S}^{2h},$$

where

$\tilde{\phi}^{2h} = I_h^{2h}\tilde{\phi}^h + e_\phi^{2h}$ and $\hat{C}^{2h} = \hat{A}^{2h}(I_h^{2h}\tilde{\phi}^h) - \hat{S}^{2h} + I_h^{2h}R^h$.

The term $\hat{C}^{2h}$ is kept constant during the iteration. It should be noted that $\hat{S}^{2h}$ and $\tilde{S}^{2h}$ were identical at the first iteration, as the iterations have progressed, they will differ each other resulting in driving a coarse grid iteration process. The restricted residual and the different in source terms behave like the source-driving term. Thus the coarse grid equation is the source-driven procedure. Subsequently, having a required little iteration at coarser grid finished, the correction is calculated using the following formula:

$$e_\phi^{2h} = \tilde{\phi}_{new}^{2h} - \tilde{\phi}_{old}^{2h} = \tilde{\phi}_{new}^{2h} - I_h^{2h}\tilde{\phi}^h.$$

Hence the correction is transferred back to the finest grid, this is the prolongation process. Then the finest grid solution is corrected there using the prolonged correction as follows:

$$\tilde{\phi}_{new}^h = \tilde{\phi}_{old}^h + I_{2h}^h e_\phi^{2h}.$$

Up to now, one multigrid V-cycle is complete. This version of multigrid method is the full approximation storage (FAS) scheme in which the approximate solution at fine grid is also restricted onto the coarser grid, not only the residual. The restriction and prolongation are done by bi-linear interpolation for the field variables, but different approach for the residuals, which are restricted by area, weight-averaged. In this paper, however, even the turbulent quantities are restricted to the coarse grids; they are not solved there and the correction process is not performed, they are used to calculate the eddy viscosity at the coarse grids only. Special treatment should be carefully done for the calculation of turbulent quantities at the coarse grids to avoid being negative value, usually physical non-negative value.

5. Results and Discussion

The two main issues considered in this work are the multigrid efficiency and the accuracy of each turbulence model used. The multigrid efficiency is first investigated here because all the computed results are obtained with the use of multigrid computation. The finest grid contains 160x160 number of grid points and four levels of grid are used in all cases. Fig. 1-3 show the residual histories in the calculation by using the k-ε model, the k-ω-SST model and the $\overline{v^2}$-f model respectively. Among these results, it is found that the multigrid technique exhibits very high efficiency for the simulation in the LS model. The respective degradations in efficiency are observed for the SST and V2F models. The LS model cannot be estimated the portion of computing time that could be reduced, because the converged state of single grid computation could not be obtained. The multigrid technique can save the computing time by 3 hours for the SST model and 1 hour 30 minutes for the V2F model. Obviously the efficiency of the multigrid technique performed in the SST model is higher than that performed in the V2F model. It should be noted that the eddy viscosity relation in the SST model is also associated with the velocity components, whereas in the V2F model the eddy viscosity is only related to the turbulent quantities. Since the velocity components are updated every multigrid cycles, this leads to the update in the eddy viscosity for the SST turbulence model resulting in faster convergence rate. On the other hand, the residual reduction oscillates strongly for the single computation of the SST model, while the V2F model is rather smooth. Therefore, this can be revealed that the V2F turbulence mode is more stable than the SST turbulence model.

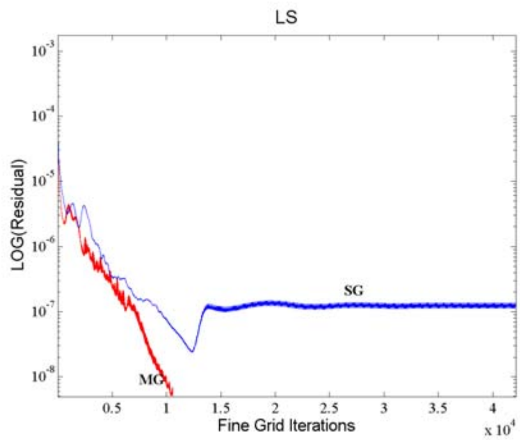

Figure 1. Residual reductions in the Launder & Sharma turbulence model by using single grid and multigrid.

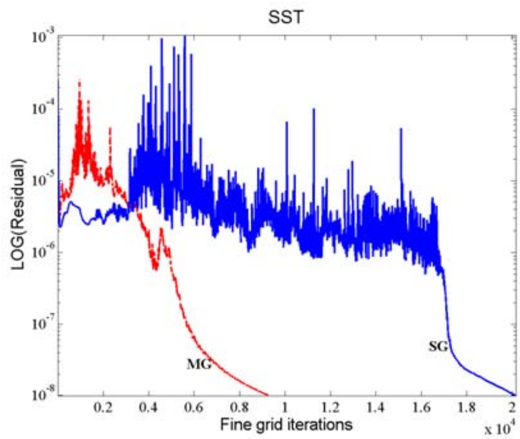

Figure 2. Residual reductions in the SST-k-ω turbulence model by using single grid and multigrid.

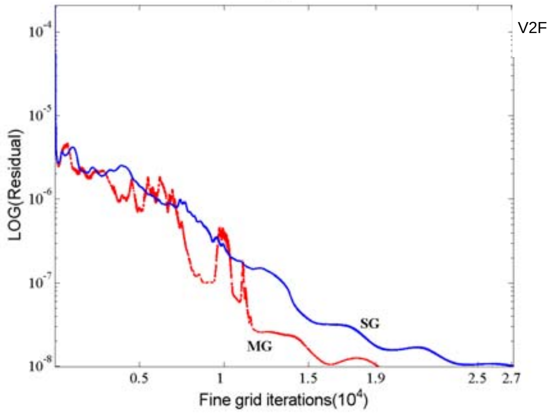

Figure 3. Residual reductions in the $\overline{v^2}$-f model using single grid and multigrid.

Although the multigrid technique has gained in highest efficiency for the LS model computation, but the required converged solutions turn out to have lowest accuracy. As shown in Fig. 4, the SST and V2F models can predict correctly the vertical velocity profile along the horizontal centered line of a cavity, which are in good agreement the experimental data, while the LS model is poor in predicting the velocity profile. In Fig. 5 (a) and (b), the velocity profiles near vertical walls are enlarged for clearly viewing. It is found that the V2F model has better accuracy than the SST model.

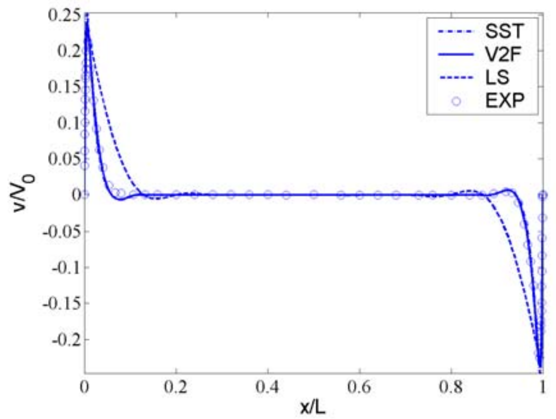

Figure 4 Profile of vertical velocity component along the middle horizontal line.

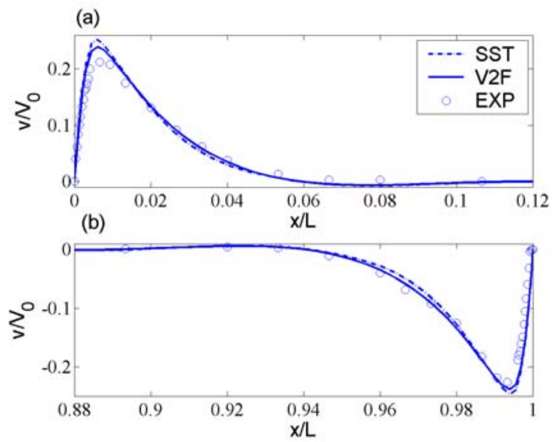

Figure 5 Enlargement of velocity profiles in the vicinity of (a) left and (b) right vertical walls.

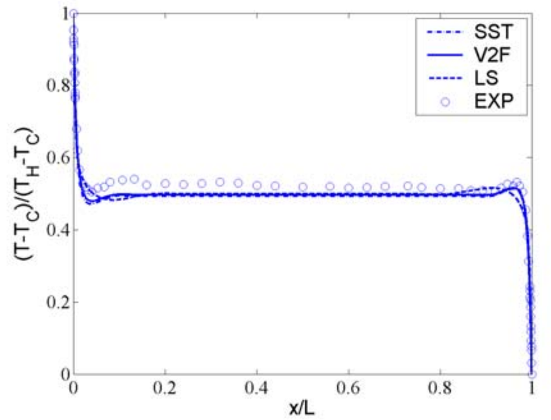

Figure 6 Temperature profile along the middle horizontal line.

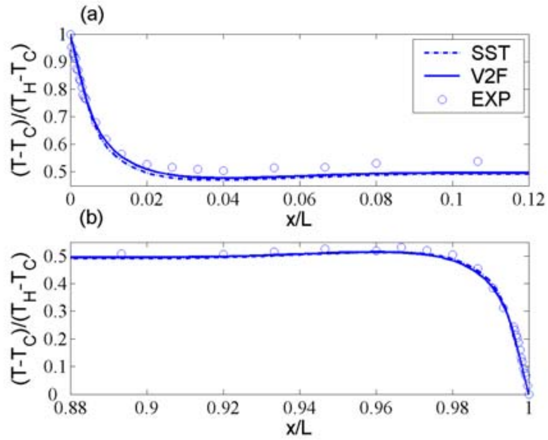

Figure 7 Enlargement of temperature profile in the vicinity of (a) left and (b) right vertical walls.

The temperature profiles along the horizontal centered line of a cavity are shown in Fig. 6. Again the LS model is poor to predict the temperature profile, in particularly adjacent to the wall. In Fig. 7 (a) and (b), the profiles are enlarged in the vicinity of the wall. The V2F model can predict slightly better than the SST model does. It is found that all models underestimate the temperature in the core region. This might have been arisen by an excessive heat transfer at the bottom wall causing from an improper boundary condition for the two non-isothermal horizontal walls.

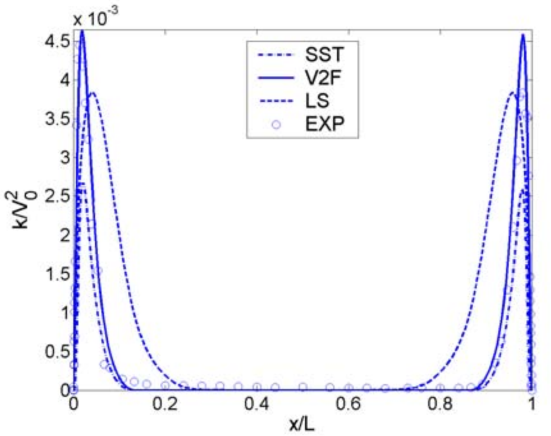

Figure 8 Turbulent kinetic energy profiles along the middle horizontal line.

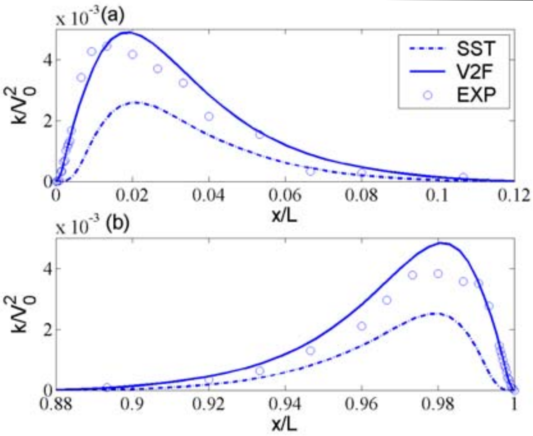

Figure 9 Enlargement of turbulent kinetic energy profile in the vicinity of (a) left and (b) right vertical walls.

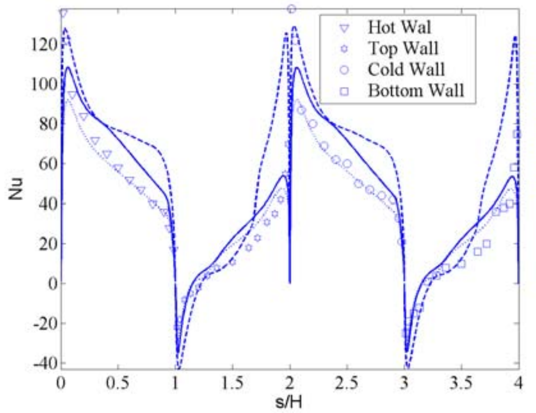

Figure 10 Local Nusselt number along the walls: symbols (EXP), dash-dash (LS), solid (V2F) and dot-dot (SST).

The profiles of turbulent kinetic energy along the horizontal centered line of a cavity are shown in Fig. 8. As shown previously, the trend remains the same. The LS model fails to predict correctly the turbulent kinetic energy and the SST and V2F models are in good agreement with the experimental data. The enlarged views in the vicinity of the walls are shown in Fig. 9 (a) and (b). Obviously, the V2F model slightly over-predicts the turbulent kinetic energy, while the SST model substantially under-predicts the one. The predictions of heat transfer are shown in Fig. 10 via the local Nusselt number *Nu* along the wall. The abscissa *s/H* denotes a length along the cavity walls in the clockwise direction, where *s/H = 0* and *s/H = 4* are at the left-bottom corner. As the results shown, the SST model gives the best result among all models even it under-predicts the peak value of *Nu*. Even if the LS model can nearly predict the peak value of *Nu* over the other models, but in overall prediction, it over-predict too much, in particularly at the right-top and left-bottom corners.

As just discussed above, it seems that the V2F model is the best one in predicting turbulent natural convection in a square enclosure, which can be noticed from its capability in predicting the velocity, temperature and turbulent kinetic energy profiles much accurately. In addition, there is one issue regarding the relaminarization of solution, which is often encountered for certain two-equations low-Re-number turbulence model. Then an additional attempt made in this work performs by lowering the required convergence point, i.e. lowering below 10^{-8}. The results demonstrate something very interesting. The V2F model immediately becomes relaminarization, but the SST model does not. The computed results of the SST model are rather unchanged. In regard to the LS model simulation, the residual can be reduced only one order from here and then behaves like the residual history of a single grid, i.e. displaying the horizontal line one order below the single grid residual line; moreover, the improvement in solutions can not be observed.

6. Conclusions

This paper presents the implementation of a multigrid technique into the three low-Re-number two-equations turbulence models. The turbulence models used in this work are the k-ε turbulence model of Launder and Sharma (LS), the k-ω-SST turbulence model of Menter (SST), and the $\overline{v^2}$-f turbulence model of Durbin (V2F). The tested problem with geometric simplicity but complexity in flow selected in this work is a natural convection in a square enclosure. The results show that the multigrid technique exhibits the highest efficiency for the simulation using the LS turbulence model. The degradations in efficiency are found in the SST and V2F turbulence models respectively. In contrast, at the required convergence point, the LS model gives the worse accurate solutions, but the V2F model gives the best accurate ones, while the solutions accuracy of the SST model are slightly lower than an accuracy of the V2F model. In other words, with lowering the required convergence point below the one set before, the V2F model immediately gives the laminar solution, while the SST model gives the unchanging solutions and the improvement in solutions of the LS model cannot be found. In heat transfer prediction, the SST model can predict more accurate than the other models. With several reasons, this can be concluded that the k-ω-SST turbulence model is more suitable to simulate the turbulent natural convection in an enclosure.

Acknowledgments

This research work is partly supported by the Thai National Grid Project. The financial support from the Thailand Research Fund (TRF) for the Senior Scholar Professor Pramote Dechaumphai is also acknowledged

References

[1] Launder, B.E. and Sharma, B, 1974. Application of Energy Dissipation Model of Turbulence to the calculation of Flow near a Spinning Disk. Letters in Heat and Mass Transfer. Vol. 1, No. 2, pp. 131-138.
[2] Menter, F.R., 1994. Two-Equations Eddy-Viscosity Turbulence Models for Engineering Applications. AIAA Journal, Vol. 32, No. 8, pp. 1598-1605.
[3] Durbin, P.A., 1995. Separated Flow Computations with the $k-\varepsilon-\overline{v^2}$ Model. AIAA Journal, Vol. 33,

pp. 659-664.

[4] Ampofo, F. and Karayiannis, T.G., 2003. Experimental Benchmark Data for Turbulent Natural Convection in and Air filled Square Cavity. International of Journal of Heat and Mass Transfer, Vol. 46, pp. 3551-3572.

[5] Liu, F. and Wen, J.X., 1999. Development and Validation of an Advanced Turbulence Model for Buoyancy Driven Flows in Enclosures. International Journal of Heat and Mass Transfer, Vol. 42, pp. 3967-3981.

[6] Iaccarino, G., 2001. Predictions of a Turbulent Separated Flow Using Commercial CFD Codes. ASME Journal of Fluids Engineering, Vol. 123, pp. 819-828.